energies

MDPI

Article

Efficiency Optimization Design of L-LLC Resonant Bidirectional DC-DC Converter

Jing Lu [1], Xiangqian Tong [1,*], Jianwu Zeng [2], Ming Shen [1] and Jun Yin [1]

[1] School of Electrical Engineering, Xi'an University of Technology, Xi'an 710048, China; lujing@stu.xaut.edu.cn (J.L.); sunmoon@xaut.edu.cn (M.S.); yyinjun@xaut.edu.cn (J.Y.)
[2] Department of Electrical and Computer Engineering & Technology, Minnesota State University, Mankato, MN 56001, USA; jianwu.zeng@mnsu.edu
* Correspondence: lstong@mail.xaut.edu.cn

Abstract: The new type of L-LLC resonant bidirectional DC-DC converter (L-LLC-BDC) has merits of high efficiency, high-power density and wide gain and power ranges, and it is suitable for energy interface between energy storage systems and DC micro grid. However, the resonances are sensitive to the parasitic parameters, which will deteriorate the efficiency. This paper investigates the intrinsic mechanism of parasitic parameters on the L-LLC-BDC operating principle and working characteristics based on the analysis of working modes and resonance tank. By taking the oscillation of parasitic parameters produced in the stage for the freewheeling stage into consideration, a parameter optimization method is proposed to reduce the resonant current oscillation while maintaining the characteristic of the natural soft switching. The experiment results not only validated the proposed parameter optimization design method, but also testified to the improvement of the efficiency through the minimization of the conduction and switching loss.

Keywords: L-LLC-BDC; resonant parameters; optimization design; mode analysis; MOSFET output capacitance

Citation: Lu, J.; Tong, X.; Zeng, J.; Shen, M.; Yin, J. Efficiency Optimization Design of L-LLC Resonant Bidirectional DC-DC Converter. *Energies* **2021**, *14*, 3123. https://doi.org/10.3390/en14113123

Academic Editor: Ambrish Chandra

Received: 28 March 2021
Accepted: 19 May 2021
Published: 27 May 2021

1. Introduction

The energy storage systems (ESSs) in the DC micro grid have a wide range of output voltages and currents, which requires a bi-directional DC-DC converter with a wide range of voltage gain and power receptivity. L-LLC resonant bidirectional DC-DC converter (L-LLC-BDC) can be used as the key equipment for interaction between ESSs and the DC micro-grid for stabilization of the DC bus voltage.

In the literature [1], the additional inductance is added to the traditional LLC resonant converter to form L-LLC-BDC, enabling a symmetrical topology that can work in both the forward and reverse directions. As this converter's operating characteristics not only depend on its working point, but also its working frequency and load condition as well, it is difficult to analyze. Ref. [2] redesigned the converter with the fundamental harmonic approximation, and the resonant voltage and current are proximately equivalent to sinusoidal waveform at resonant frequency. However, the low approximation accuracy at those points outside the resonance point cannot meet the requirements, and the gain formula obtained is deviated from the actual values to some extent. Although the parameters of the converter are designed, the key parameters are empirical values, and the design method is difficult to popularize and apply. In practical application, due to the influence of parasitic parameters, the real resonant frequency is deviated from the theoretical value, and the operating characteristics of the converter will be different from the theoretical analysis as well. Methods such as the third harmonic approximation and extended describing function are used to improve the accuracy of analysis [3,4]. However, the analytic solutions are in nature obtained through approximation.

In order to improve the efficiency of the traditional LLC resonant converter, other methods are used, e.g., optimal control strategy [5–7], optimization of the dead time and magnetic inductance [8], and peak gain method [9,10]. Recently, the new design method considering peak gain is proposed [11,12], the LLC resonant converter will get the peak gain point when the input square-wave voltage is synchronous with the resonant current. A modified gain model and its corresponding design method for LLC resonant converter are proposed [13], in which both resonant and load factor are considered and discussed in detail by combining time and frequency domain together. As complete charging and discharging within the dead time, it is necessary for the converter to achieve soft switching, then influence of the output capacitance of the switch should be taken into consideration [14–17]. The existing literature usually considers the output capacitance of the primary side switch, but rarely the secondary side capacitance. Ref. [18] proposes a primary side switch in parallel with the capacitance to mitigate the problem of the high output voltage under light load condition. Ref. [19] analyzes the output voltage oscillation caused by the parasitic capacitance of the rectifier side diode under different switching frequencies for the center-tapped LLC converter, and they proposed a new parameter design idea, which has certain limitations. Ref. [20] proposed a new topology of LLC to improve the efficiency with the increase of components; however, the power flow was unidirectional. The more accurate time domain analysis was adopted in [21–25].

Based on an accurate time domain analysis of the L-LLC-BDC operation process, this paper proposes a parameter optimization design method, which takes into account the effect of the output capacitance of the switch. The proposed method effectively eliminated the current oscillation when switches turn on by configuring switching frequency, the conduction and switching loss of the converter are reduced by larger magnetizing inductance of the converter on the basis of satisfying the voltage gain of the converter. The efficiency is increased.

This paper is organized as follows: Section 2 introduces the working principle of the Bi-directional L-LLC resonant converter; Section 3 describes the time-domain analysis of the converter; Section 4 proposed a parameter optimization design; Section 5 provides the experimental results, and Section 6 concludes this paper.

2. Working Principle of the L-LLC Resonant Bi-Directional DC-DC Converter

Figure 1 shows the topology of L-LLC-BDC, whose primary and secondary sides are connected to a full-bridge converter, respectively. Where V_{in} and V_O represent the voltage of ESSs and the DC bus, respectively, L_{m1} represents magnetizing inductance of the transformer, L_r and C_r are resonant inductor and capacitor, and L_{m2} is the additional inductor. S_1–S_4 and S_5–S_8 are switches on the primary and secondary converter, respectively. D_1–D_8 and C_1–C_8 are body diodes and output capacitors corresponding to S_1–S_8. As indicated in Figure 1, the forward power direction is defined as from the primary side to the secondary side. To simplify the analysis as well as control, L_{m2} is set the same as L_{m1} so that the working principles in forward and reverse power direction are exactly the same. Therefore, only the working principle analysis in the forward mode is provided. In the forward mode, the output voltage is regulated with the frequency modulation method. When the converter works in the continuous conduction mode, L_r and C_r form a resonant tank, while in the discontinuous conduction mode, L_{m1} and L_{m2} participates the resonance in the forward and reverse mode, respectively. For example, in the forward mode, the L_{m2} does not participate in the resonance, but it helps the switches on the primary-side switch to realize ZVS. Therefore, so does L_{m1} in the reverse mode.

Considering the influence of the MOSFET output capacitor on the working process of L-LLC-BDC, Figure 2 is intended to show the main steady-state waveforms of the converter, according to the status of the switches, and there are a total 6 modes. Due to the symmetric waveforms in the positive and negative period, the working principles in these periods are similar, only the analysis in the first half of the cycle is provided in this paper. The primary side currents are $i_p = i_{Lr} + i_{Lm2}$ and $i_s = n\,(i_{Lr} - i_{Lm1})$.

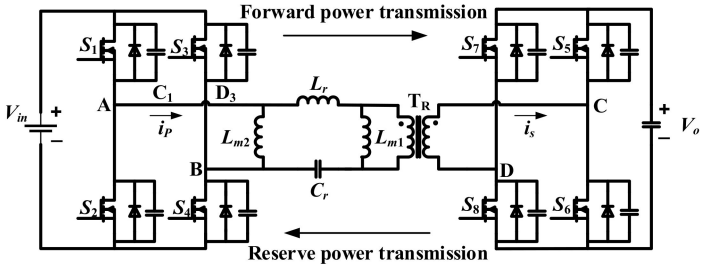

Figure 1. The circuit topology of L-LLC-BDC.

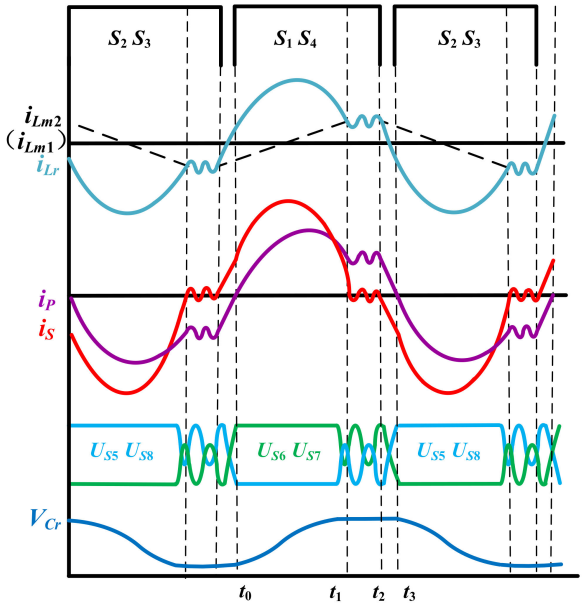

Figure 2. The main steady-state waveforms of the converter.

2.1. Mode I

Mode I: $t \in [t_0, t_1]$ (see Figure 2), during which switches S_1 and S_4 are turned on. Before t_0, the output capacitors of the switches S_1 and S_4 discharge to zero voltage through i_p, thus the switches S_1 and S_4 can be turned on under the ZVS condition, $v_{AB} = V_{in}$. The body diodes of the secondary side switches S_5 and S_8 are conducted, which clamping $v_{CD} = V_O$ energy is delivered to the load.

2.2. Mode II

Mode II: $t \in [t_1, t_2]$ (see Figure 2), during which switches S_1 and S_4 are still turned on, L_r and L_{m1} resonate with C_r, the resonant current is equal to the magnetizing current and the secondary side current i_s is zero. With the current being zero, the body diodes D_5 and D_8 are shut off naturally without reverse recovery loss, realizing ZCS of the secondary switch. The output voltage no longer clamps the two points of C–D, and the output capacitor C_5–C_8 participate in the resonance. This mode is actually a continuous current stage.

2.3. Mode III

Mode III: $t \in [t_2, t_3]$ (see Figure 2), during which switches S_1 and S_4 are off, entering into the dead time. The i_p charges the C_1 and C_4 until their voltage reach to V_{in} meanwhile. C_2 and C_3 discharges and their voltage drops to zero, which enables S_2 and S_3 to be turned on under the ZVS condition. The secondary current i_s charges C_5 and C_8 to a voltage of V_O, and the voltage S_6 and S_7 decreases to zero. At the end of this stage, after the charging and discharging, the voltage at A–B is $-V_{in}$, and the voltage at C–D is clamped at $-V_O$. Figures 3–5 show the equivalent circuits for Modes I, II and III and the differential

equations are established, respectively, and we can get the expression of resonant inductor current and resonant capacitor voltage.

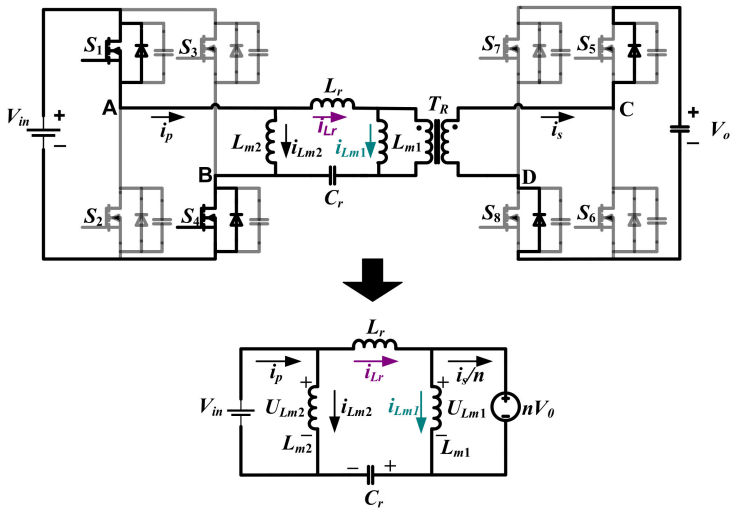

Figure 3. Resonant operation Mode I and equivalent circuit of L-LLC-BDC.

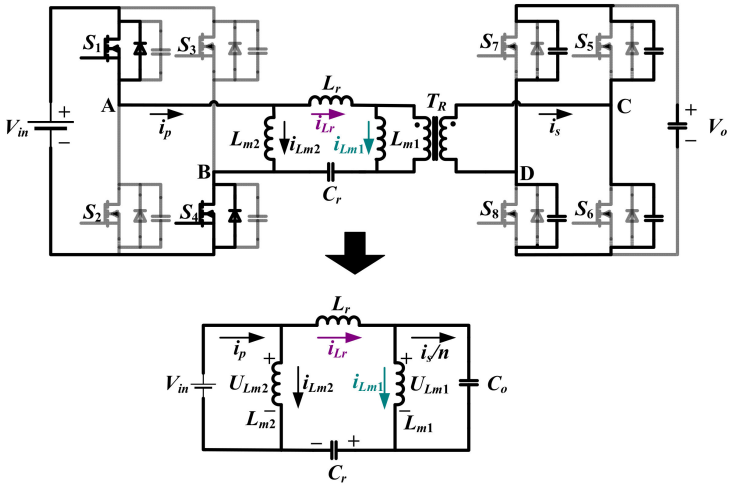

Figure 4. Resonant operation Mode II and equivalent circuit of L-LLC-BDC.

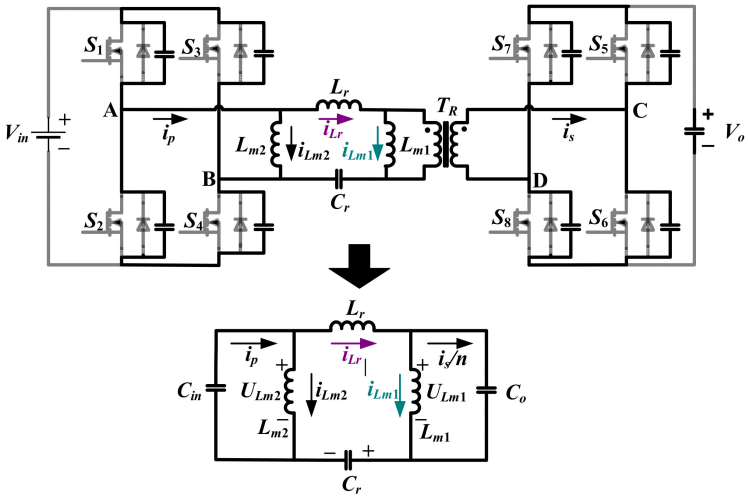

Figure 5. Resonant operation Mode III and equivalent circuit of L-LLC-BDC.

3. The Time-Domain Analysis of L-LLC Resonant Bi-Directional DC-DC Converter

The first harmonic approximation (FHA) only considers the component at the fundamental frequency, while the high order harmonics are neglected, which makes it lack the capability to identify different operating modes. Therefore, it is necessary to build an accurate steady-state model to describe the converter's operating process and characteristics. In the period of Mode II, the output capacitor of the secondary side switch participates in resonance, and the four output capacitors are connected in series in pairs and then in parallel, which can be then equivalent to the capacitance C_o. In the Mode III, which corresponds to the dead time, $C_1 \sim C_4$ and $C_5 \sim C_8$ are connected in series in pairs and then in parallel, equivalent to the capacitor C_{in} and C_o, respectively. Due to the short time of Mode III, both i_{Lm1} and i_{Lm2} can be taken as unchanged. With the simplified circuit and initial conditions of each resonant operating mode in Figures 3–5, the voltage of the resonant capacitor, i.e., u_{Cr}, i_p as well as i_s can be obtained in each mode.

3.1. Mode I

The time-domain expression of Mode I:

$$\begin{cases} u_{Cr}(t) = I_{Lr0}Z_0\sin[\omega_0(t-t_0)] + [U_{Cr0} - (V_{in} - V_O)]\cos[\omega_0(t-t_0)] + V_{in} - nV_O \\ i_P(t) = I_{Lr0}\cos[\omega_0(t-t_0)] + \frac{[U_{Cr0}-(V_{in}-V_O)]}{Z_0}\sin[\omega_0(t-t_0)] + \frac{V_{in}}{L_{m2}}(t-t_0) - I_m \\ i_s(t) = nI_{Lr0}\cos[\omega_0(t-t_0)] + \frac{[U_{Cr0}-(V_{in}-V_O)]}{Z_0}n\sin[\omega_0(t-t_0)] - \frac{nV_{in}}{L_{m2}}(t-t_0) + nI_m \end{cases} \quad (1)$$

where, I_{Lr0} and U_{cr0} are the current of resonant inductor L_r and voltage of the capacitor C_r at time t_0, respectively; I_m represents the peak current of magnetizing inductance L_{m1} and additional inductance L_{m2}; Z_0 the characteristic impedance, the initial value of the voltage of resonant capacitor at time t_0, and ω_0 is the resonant frequency, which can be calculated as follows:

$$Z_0 = \sqrt{L_r/C_r}\omega_0 = \frac{1}{\sqrt{L_rC_r}}$$

3.2. Mode II

The time-domain expression of Mode II:

$$\begin{cases} u_{Cr}(t) = A_1\cos(\omega_{11}t) + A_2\sin(\omega_{11}t) + A_3\cos(\omega_{12}t) + A_4\sin(\omega_{12}t) + V_{in} \\ u_{C_O}(t) = (\frac{C_r(L_{m1}+L_r)-L_{m1}nC_O}{L_{m1}nC_O})[A_1\cos(\omega_{11}t) + A_2\sin(\omega_{11}t)] - \frac{L_{m1}}{L_r+L_{m1}}[A_3\cos(\omega_{12}t) + A_4\sin(\omega_{12}t)] \\ i_s(t) = \omega_1\frac{(L_{m1}+L_r)C_r}{L_{m1}}[-A_1\sin(\omega_{11}t) + A_2\cos(\omega_{11}t)] - \omega_2\frac{L_{m1}C_{oss1}}{L_r+L_{m1}}[-A_3\sin(\omega_{12}t) + A_4\cos(\omega_{12}t)] \\ i_p = C_r\omega_1[-A_1\sin(\omega_{11}t) + A_2\cos(\omega_{11}t)] + C_r\omega_2[-A_3\sin(\omega_{12}t) + A_4\cos(\omega_{12}t)] + \frac{nV_O}{L_m}(t_2-t_1) - I_m \end{cases} \quad (2)$$

where, A1, A2, A3 and A4 are

$$A_1 = \frac{L_{m1}^2}{(L_{m1}+L_r)^2}\frac{nC_O}{C_r}[U_{Cr1} - V_{in}] + \frac{L_{m1}nC_O}{C_r(L_{m1}+L_r)}U_{C_{O1}}$$

$$A_2 = \frac{L_{m1}nC_OI_{Lr1}}{(L_{m1}+L_r)^2C_r^2\omega_{11}}$$

$$A_3 = U_{Cr1} - V_{in} - \frac{L_{m1}nC_O}{(L_{m1}+L_r)C_r}u_{C_{O1}}$$

$$A_4 = \frac{I_{Lr1}}{C_r\omega_{12}}$$

where $t_1 < t < t_2$, I_{Lr1} is the initial value of the current of resonant inductor at time t_1, U_{Cr1} the initial value of the voltage of resonant capacitor at time t_1, and U_{Co1} the initial value of the voltage of output capacitor at time t_1.

$$\omega_{11} = \frac{1}{\sqrt{\frac{L_rL_{m1}nC_o}{L_{m1}+L_r}}}$$

$$\omega_{12} = \frac{1}{\sqrt{(L_{m1}+L_r)C_r}}$$

3.3. Mode III

Since the dead time is very short, it can be considered that in this period both current of magnetizing inductance L_{m1} and additional inductance L_{m2} are constant at I_m. The voltage of the equivalent capacitor C_{in} and C_o are constant at U_1 and U_2, respectively.

The time-domain expression of Mode III:

$$\begin{cases} u_{Cr}(t) = I_{Lr2}Z_2\sin[\omega_2(t-t_2)] + [U_{Cr2} - (U_1 - U_2)]\cos[\omega_2(t-t_2)] \\ i_p(t) = I_{Lr2}\cos[\omega_2(t-t_2)] - \frac{U_{Cr2}-(U_1-U_2)}{Z_2}\sin[\omega_2(t-t_2)] + I_m \\ i_s(t) = nI_{Lr2}\cos[\omega_2(t-t_2)] - \frac{U_{Cr2}-(U_1-U_2)}{Z_2}n\sin[\omega_2(t-t_2)] - nI_m \end{cases} \quad (3)$$

In the expression, I_{Lr2} is the initial value of the resonant inductor current at time t_2, and U_{Cr2} the initial value of the resonant capacitor voltage at time t_2. Z_2 represents the characteristic impedance, and ω_2 the resonant frequency.

$$Z_2 = \sqrt{L_r/C_r}\omega_2 = 1/\sqrt{L_rC_r}$$

During this period, the switches S_1–S_4 are all turned off, i_p and i_s are charged and discharged C_1–C_4 and C_5–C_8, respectively. The operating principle is shown in Figure 6 below.

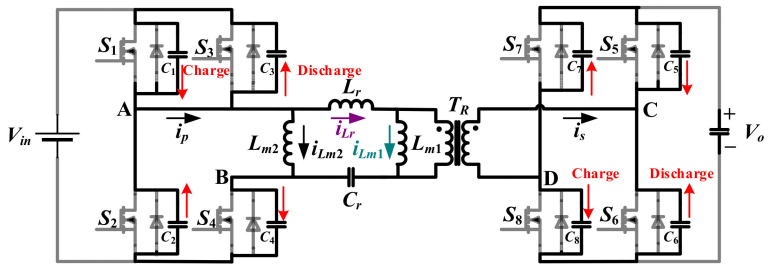

Figure 6. The operation mechanism for the dead time.

The voltage expressions of $u_{C2}(t)$ and $u_{C6}(t)$ in this period can be obtained.

$$\begin{cases} u_{C2}(t) = \frac{1}{2\omega_2C_2}I_{Lr2}\sin[\omega_2(t-t_2)] + \frac{U_{Cr2}-(U_1-U_2)}{2Z_2\omega_2C_2}\cos[\omega_2(t-t_2)] + \frac{I_m(t-t_2)}{2C_2} + V_{in} \\ u_{C6}(t) = \frac{1}{2\omega_2C_6}I_{Lr2}\sin[\omega_2(t-t_2)] + \frac{U_{Cr2}-(U_1-U_2)}{2Z_2\omega_2C_6}\cos[\omega_2(t-t_2)] - \frac{I_m(t-t_2)}{2C_6} + nV_o \end{cases} \quad (4)$$

4. The Parameter Optimization Design of L-LLC Resonant Bi-Directional DC-DC Converter

It can be seen from Figure 2 and the mathematical analysis for each working mode that the output capacitor of the switch participates in the operation of the circuit only in Mode II and III. When $t_1 < t < t_2$, v_{CD} is no longer clamped to V_O, the output capacitors of the switches and L_{m1} form a resonant tank, which results in the high frequency oscillation at both primary and secondary side switches. Such, oscillation not only increases the conduction loss of the switch, but also affects the charging and discharging of the output capacitor during the dead time., i.e., $t_2 < t < t_3$. At the dead time, both side switches are disconnected, C_1–C_4 and C_5–C_8 are charged by i_p and discharged by i_s, respectively. To maintain the same topology in forward and reverse modes, parameters such as the output capacitance of MOSFET are kept to be symmetric, so that capacitance referred from the secondary side is equal to that on the primary side. The decrease of the primary side current i_p will affect the soft switch of the converter. If the primary side current flows in reverse and drops the zero before the end of this period, the capacitors cannot be fully discharged, which results in the failure of the primary side switch to realize ZVS. Moreover, the change of current in dead-time makes the converter continue to a continuous current stage even when the switching frequency equals the resonant frequency.

The effect of the aforementioned output capacitor of MOSFET toward the operation of the converter can be eliminated by parameter optimization to improve the performance of the converter. The first consideration in the design of the resonant component is to reduce the loss of the converter to improve its efficiency. As L-LLC-BDC has the characteristic of the natural ZVS soft switching, the conduction loss accounts for a major part. It was testified that the current circulation can be reduced by increasing the magnetic inductance. However, there are trade-offs, with the increasing of magnetizing inductor, its current will be decreased, which prevents switches from achieving ZVS soft-switching.

As can be seen from Figure 2, the voltage variation range of the output capacitance is the largest in the dead time, large i_p and i_s are required for charging and discharging the capacitance. In practice, due to the presence of the stray inductance in the circuit, the voltage and current oscillation in the stage of Mode II are both attenuated. Therefore, the design should be based on the first zero crossing of i_s to guarantee the ZVS soft-switching. Then, there is no operating Mode II.

According to the optimization goal of L-LLC-BDC, the starting point of the proposed improvement design method is to ensure that the magnetizing current fully charges and discharges the output capacitor of the switch within the dead time T_d, so as to achieve ZVS. From u_{C2} $(t_3) = 0$, u_{C6} $(t_3) = 0$, namely

$$\begin{cases} u_{C2}(t) = \frac{1}{2\omega_2 C_2} I_{Lr2} \sin(\omega_2 T_d) + \frac{U_{Cr2}-(U_1-U_2)}{2Z_2\omega_2 C_2} \cos(\omega_2 T_d) + \frac{I_m T_d}{2C_2} + V_{in} = 0 \\ u_{C6}(t) = \frac{1}{2\omega_2 C_6} I_{Lr2} \sin(\omega_2 T_d) + \frac{U_{Cr2}-(U_1-U_2)}{2Z_2\omega_2 C_6} \cos(\omega_2 T_d) - \frac{I_m T_d}{2C_6} + nV_o = 0 \end{cases} \tag{5}$$

From Equation (5), the peak magnetizing current can be obtained:

$$I_m = \frac{2C_2 V_{in}}{T_d} \tag{6}$$

It can be seen from Equation (6) that with the selected device and given dead time, the peak magnetizing inductor current I_m can be obtained. When i_p and i_s fully charges and discharges the primary side output capacitor and secondary side capacitor of the switch within the dead time, the waveform of the converter is the same as Figure 7.

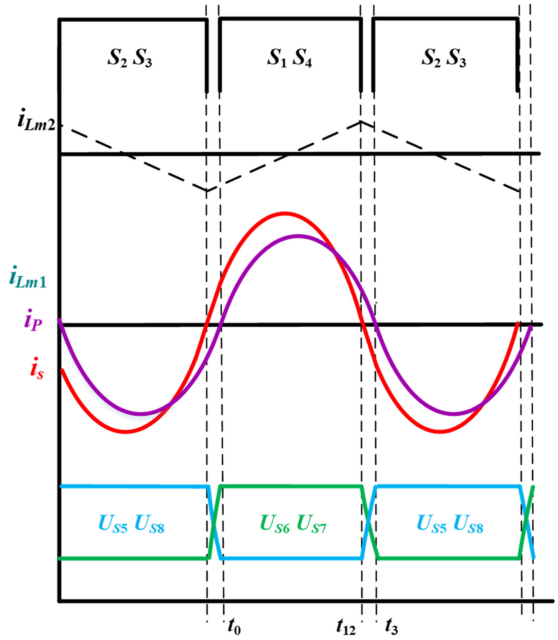

Figure 7. The working waveform under optimization design.

This is the resonant mode of the converter, and the resonant frequency is slightly higher than the resonant frequency. Under this condition, the charge and discharge of the capacitors are completed in the dead time, but due to the current on the additional inductance, the primary switch can realize ZVS completely. The resonant current has little distortion when the switch is turned on, and the expressions of the primary and secondary side current in the period T_B (from t_0 to t_{12}) can be obtained. Since the instantaneous value of i_{Lr} at time t_0 is 0, and the instantaneous value of i_{Lr} at time t_{12} is I_m, then i_s can be obtained:

$$i_s(t) = \frac{nI_m}{\sin(\omega_0 T_B)} \sin[\omega_0(t - t_0)] + nI_m - \frac{V_{in}}{L_{m1}}(t - t_0) \tag{7}$$

The field current i_{Lm1} at t_{12} in the period of Mode 1 can be linearly approximated as:

$$L_{m1} = \frac{V_{in} T_B}{4I_m} \tag{8}$$

When the converter works in the resonant mode, energy from i_s to the load within period as shown in the following expressions:

$$\frac{1}{T_B + T_d} \int_0^{T_B} i_s dt = \frac{P_O}{V_O} \tag{9}$$

$$\frac{\cos(\frac{\pi T_B}{T_0 + T_d}) + 1}{\frac{\pi}{T_0 + T_d} \sin(\frac{\pi T_B}{T_0 + T_d})} = \frac{P_O(T_B + T_d)}{nV_O I_m} \tag{10}$$

Given the resonant frequency f_0, rated power P_O, output voltage V_O and dead time T_d, the value of the period T_B from t_0 to t_{12} can be obtained. At this time, the ideal resonant frequency is $f = 1/(2T_B + 2T_d)$.

To analyze the effect of output capacitance toward the voltage gain M, simulation studies are carried under the different switching frequency with and without output capacitance. Figure 8 shows that voltage gain vs. switching frequency under the different load with the parasitic capacitance. Its characteristic curve is basically the same as that of the converter that does not consider the output capacitance. However, the gain has a sudden increase with the increase of switching frequency when there is no load or the load is very light.

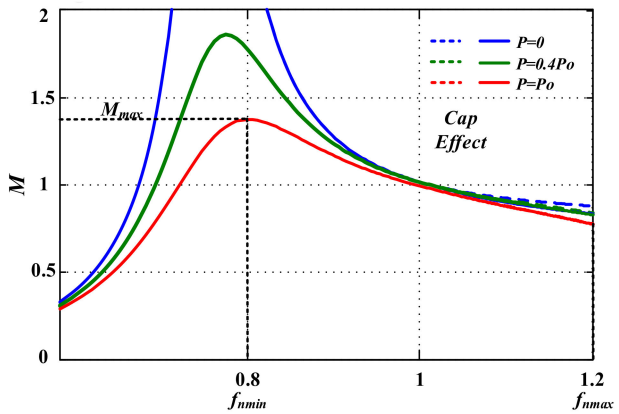

Figure 8. Effect of the parasitic capacitors on the voltage gain curve.

In order to facilitate the calculation, the gain curve can be obtained without considering the transient expression of the output capacitance. Appendix A shows the time domain equation when the converter operates at $f_s = f$, $f_s > f$, $f_s < f$, respectively. The maximum gain M can be obtained when the switching frequency f_s is the minimum.

According to reference [9], the required maximum gain expressed by the minimum and maximum input voltages U_{inmax} and U_{inmin} is the maximum gain at full load:

$$M_{\max} = \frac{U_{in\max}}{U_{in\min}} \frac{L_{m1}/L_r}{(\frac{L_{m1}}{L_r}+1)\cos(\frac{\pi f}{2\sqrt{\frac{L_{m1}}{L_r}+1} f_{\max}})} \tag{11}$$

where, M_{max} is the maximum gain which is achieved at full load when $f_s = f_{min}$. More details of M_{max} can be found in Equation (A1). U_{inmax} and U_{inmin} are the maximum and minimum input voltage, f_{max} is the maximum switching frequency.

As the L_{m1} is known, the resonant inductance ratio L_r can be calculated from Equation (11), and the resonant capacitor can be derived by the resonant frequency f_0. In practical design, the current and voltage oscillation in the continuous current stage can also be reduced by increasing the resonant capacitance value properly.

The optimum design flow is a simple mathematical expression, the design flow of L-LLC-BDC resonance parameters is shown in Figure 9.

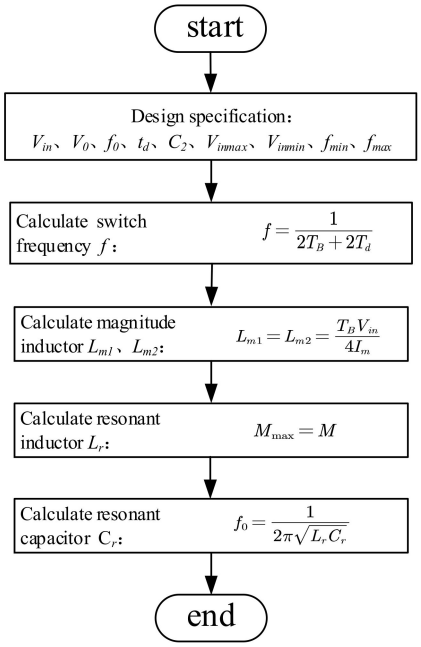

Figure 9. Flow chart of optimization design for L-LLC-BDC resonant parameters.

According to the initial conditions, the RMS current expressions of the magnetizing inductance I_p and the additional inductance I_{Lm1} and I_{Lm2} at the quasi-resonant frequency are as follows:

$$I_P = \sqrt{\frac{1}{T_B}\int_0^{T_B} i_P^2(t)dt} = \frac{V_O}{8nR_O}\sqrt{\frac{2n^4R_L^2T_B^2}{L_{m1}^2} + 8\pi^2} + \frac{T_B n V_O}{4\sqrt{3}L_{m1}} \tag{12}$$

As the ideal resonant period is less than the resonance period, i.e., $T_B < T_0$, the optimal L_{m1} (meaning the magnetic inductance is large enough) is calculated according to charging and discharging of the output capacitance of the switch in the dead time. When the output voltage and the load is constant, the effective value of the primary side current I_p and the effective values of the magnetic inductance current as shown in expressions Equation (12) will decrease, leading to improved efficiency of the converter. Even working at the other frequency, the reduced magnetizing current can also improve the efficiency of the converter.

5. Experimental Verification

To verify the optimization design method proposed in this paper, the prototype of L-LLC resonant bidirectional DC-DC converter is built. The overall experiment set-up is shown in Figure 10.

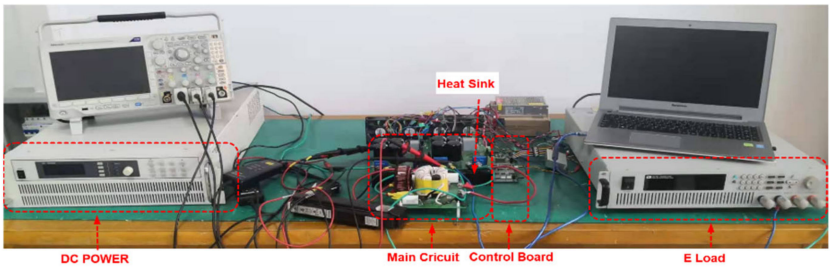

Figure 10. The experimental setup.

The input voltage varies from 630 V to 890 V, while the output voltage is 380 V. The operating frequency range is 80–120 kHz, the actual working resonant frequency f is 104 kHz, dead time is 100 ns, and output capacitor is 92 pF. A 220 pF capacitor is connected in parallel to the secondary side switch to ensure the forward and reverse topology of the converter are exactly the same. The all SiC MOSFET are mounted on the heat sink, and adopts air cooling at the same time. The comparison between parameter II before [1] and after optimization is listed in Table 1.

Table 1. The model parameters of the converter.

Symbol	Quantity	Parameter I	Parameter II
S	SiC MOSFET	C2M0080120D	C2M0080120D
V_{in}	BDC primary side rated voltage	760 V	760 V
V_o	BDC secondary side rated voltage	380 V	380 V
p	BDC rated power	6 kW	6 kW
L_{m1}	BDC magnetic inductance	0.308 mH	0.614 mH
n	BDC transformer ratio	2:1	2:1
L_r	BDC resonant inductance	0.044 mH	0.087 mH
C_r	BDC resonant capacitance	58 nF	29.1 nF
L_{m2}	BDC additional inductance	0.308 mH	0.614 mH
f	Switching frequency	100 kHz	104 kHz

To regulate the output voltage, a feedback controller is designed. Figure 11 shows the simplified control block diagram. A conventional linear regulator, such as PI compensator, controls the switching frequency to regulate the output voltage V_O to deal with the load change. The pulse frequency modulation (PFM) is applied to the converter, and the control system is built in TMS320F28335.

5.1. Steady State Waveforms

The waveforms of the voltage U_{ds1} at both ends of the primary side switch which work with the forward direction and the primary side current i_{Lr} and their detailed waveforms are shown in Figure 12. As shown in Figure 12a, when the switch is off, there is high frequency oscillation before the parameter's optimization because the capacitor of the switch is not fully charged or discharged during the dead time. It can be seen from Figure 12b that in the continuous flow stage, the output capacitance of S_1 is fully discharged in the dead time, the oscillation has been significantly reduced compare what is shown in Figure 12a, which validates the effectiveness of the parameter optimization. The waveforms of the voltage U_{ds1} at both ends of the primary side switch that work with the forward direction and the primary side current i_{Lr} and their detailed waveforms are shown in Figure 12. As

shown in Figure 12a, when the switch is off, there is a high frequency oscillation before the parameter's optimization because the capacitor of the switch is not fully charged or discharged during the dead time. It can be seen from Figure 12b that in the continuous flow stage, the output capacitance of S_1 is fully discharged in the dead time, and the oscillation has been significantly reduced compare the shown in Figure 12a, which validates the effectiveness of the parameter optimization.

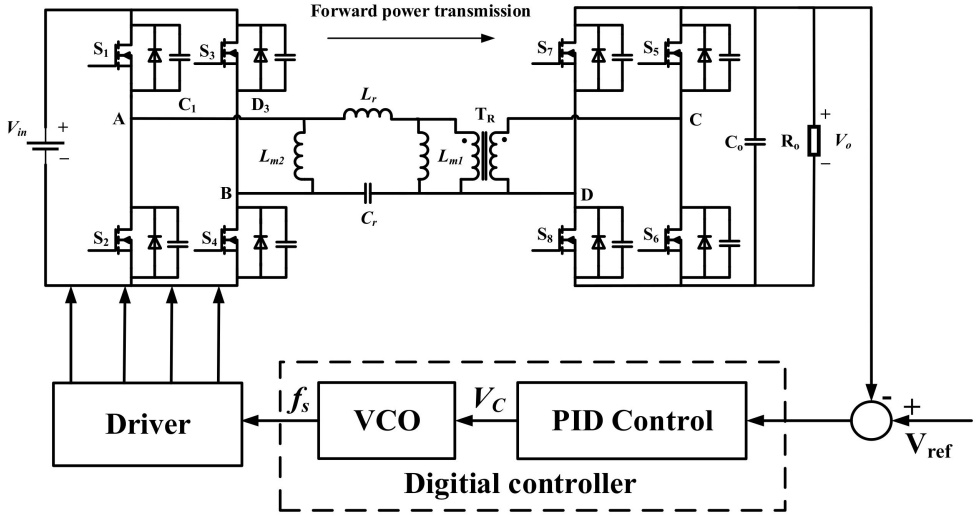

Figure 11. Control block for L-LLC resonant converter.

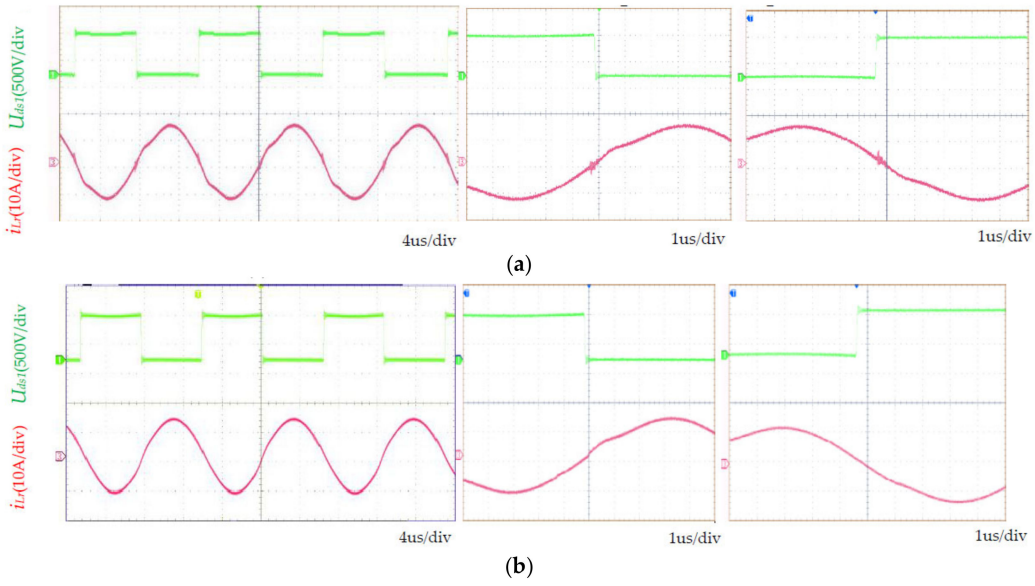

Figure 12. Comparison of the waveforms at primary side in the forward mode before and after parameter. (**a**) Before optimization. (**b**) After optimization.

5.2. ZVS Soft Switching

Figures 13–15 show the experiment waveforms with the reverse transmission when the converter is half loaded, lightly loaded, and fully loaded, respectively. Figure 13 shows the driving waveforms of switch, the waveforms of the voltage U_{ds5} at both ends of the primary side switch that works in the reverse direction at light load, the primary side current i_s, the resonant capacitor voltage U_{cr}, and their detailed waveforms. As can be seen

from Figures 13–15, the ZVS is achieved in a wide range of loads, e.g., the ZVS is achieved when the output current is 0.4 A, 4 A and 8 A.

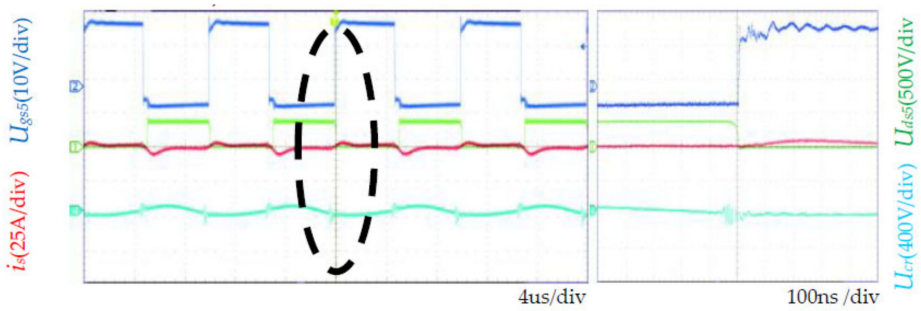

Figure 13. Test waveforms of L-LLC-BDC resonant converter at light load.

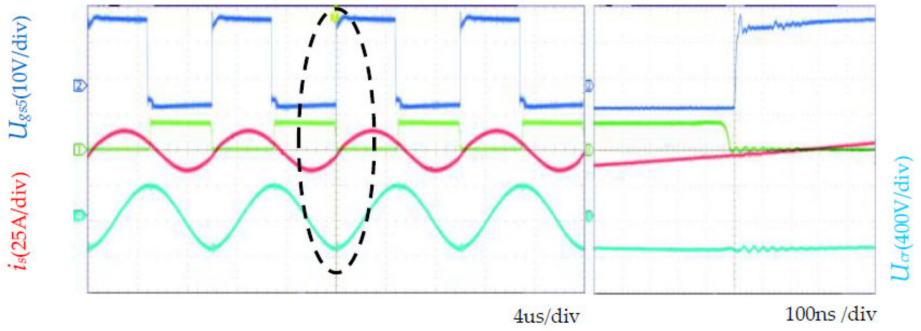

Figure 14. Test waveforms of L-LLC-BDC resonant converter at half load.

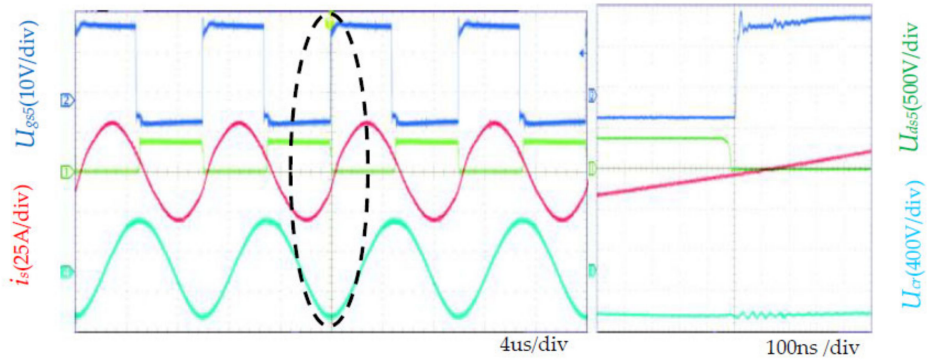

Figure 15. Test waveforms of L-LLC-BDC resonant converter at full load.

Similarly, Figure 16 compares the waveforms of the secondary side with and without optimization. U_{ds5} has oscillation in the forward direction, which is caused by the parasitic oscillation between the resonant inductor and the MOSFET parasitic capacitor when all switches are turned off after half a resonant period.

Figure 17 shows the waveforms of the voltage U_{ds5} and the secondary side current i_s when the load current is 0.4 A in forward transmission power. The waveforms of the voltage U_{ds1} of the secondary side switch S_1, and the secondary side current i_P when the load current is 0.4 A in reverse transmission power is shown in Figure 18. It can be seen that both voltage and current oscillations are decreased with forward transmission and reverse transmission significantly after the optimization.

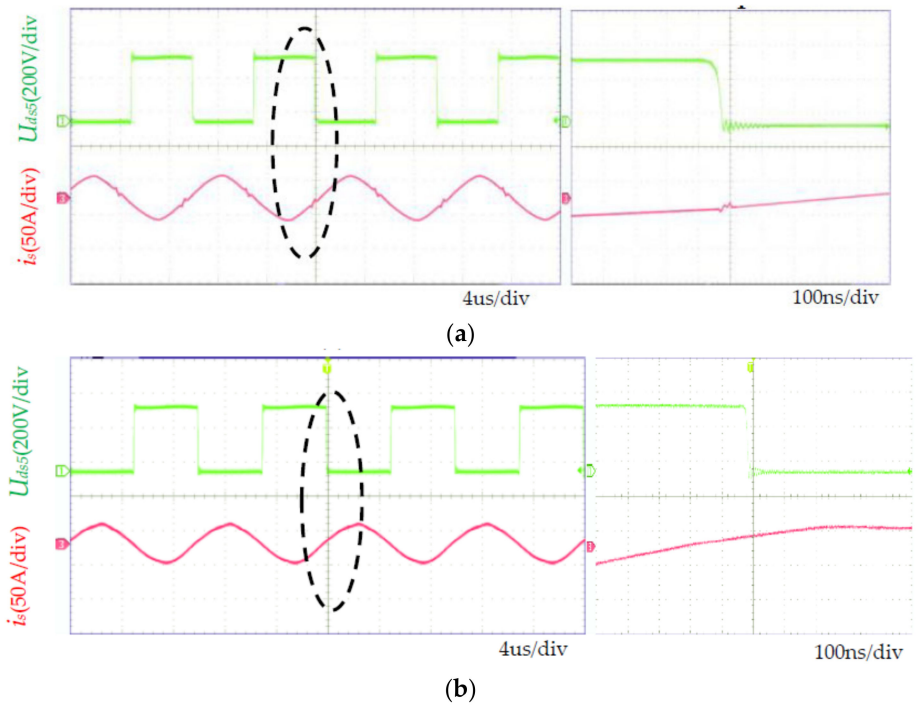

Figure 16. Experimental waveforms at the secondary side under full load with forward transmission power. (**a**) Before optimization. (**b**) After optimization.

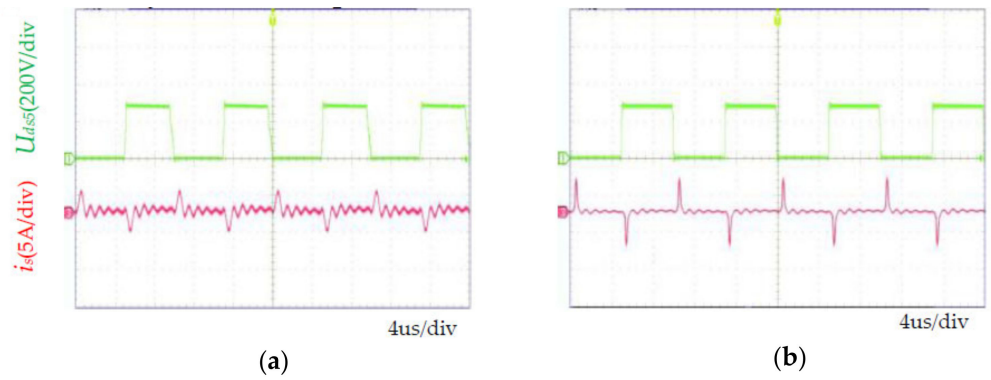

Figure 17. Experimental waveforms at secondary side under light load with forward transmission power. (**a**) Before optimization. (**b**) After optimization.

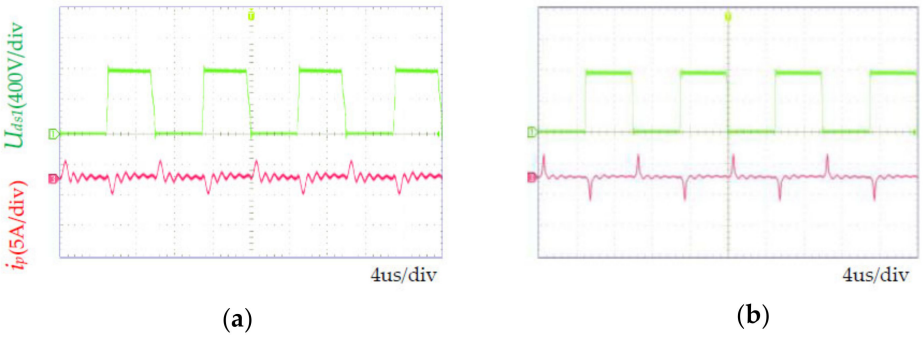

Figure 18. Experimental waveforms at secondary side under light load with reverse transmission power. (**a**) Before optimization. (**b**) After optimization.

5.3. Dynamic Waveforms

Figures 19 and 20 show the waveforms of the output voltage and the resonant current i_{Lr} when load step-up and step-down with forward transmission power by PID closed-loop control. The pulse frequency modulation (PFM) is applied to the converter, the control system is built in TMS320F28335, and control the switching frequency to regulate the output voltage V_O. According to the figure, the output voltage is constant at 380 V, indicating that L-LLC resonant bidirectional DC-DC converter has the ability to keep the output voltage constant under different loading conditions.

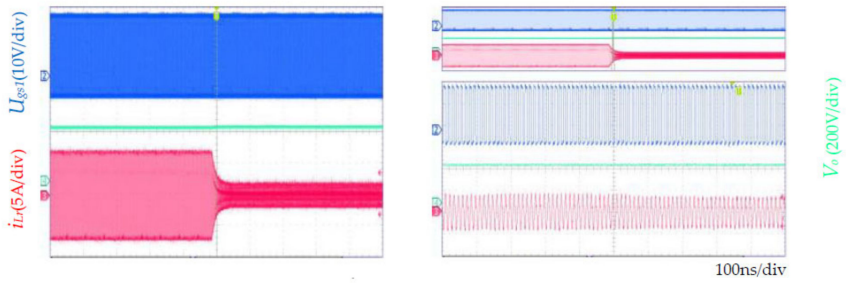

Figure 19. Dynamic response (from 3 A–12 A) when load step-up with forward transmission power.

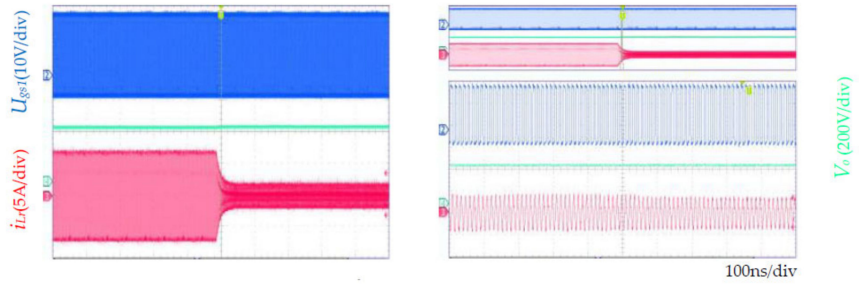

Figure 20. Dynamic response (from 12 A–3 A) when load step-down with forward transmission power.

In order to carry out a bi-directional power transmission experiment, the control block diagram of charging and discharging battery experiment system is designed, as shown in Figure 21. When the reference current is −10 A, the DC power supply charges the battery, the converter operates in forward power transmission. When the reference current is 10 A, the battery is discharged to the DC power supply, and the converter runs in reverse. The dynamic waveforms of the charging and discharging battery are shown in Figure 22. The figure shows that the charge and discharge current can follow the reference, and forward and reverse power flow can be achieved.

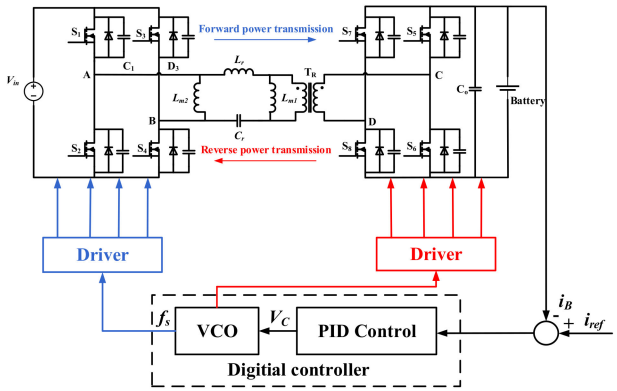

Figure 21. Bi-directional control block for L-LLC resonant converter.

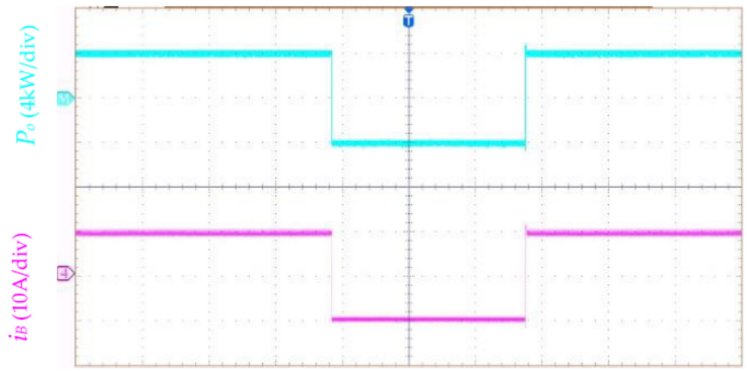

Figure 22. The dynamic waveforms of charging and discharging battery using L-LLC resonant converter.

5.4. Efficiency

The operation efficiency is measured by a power analyzer under different input voltage levels and load conditions, and electronic load is used for load regulation. Figures 23 and 24 show the efficiency curves of the design method under different loading conditions with forward and inverse transmission power. As can be seen from Figure 23 especially, when the output power is 3 kW, the maximum efficiency of the experimental device can reach up to 94.9% with forward transmission power. The design method that has been optimized delivers improved loading efficiency compared with that in the literature [4]. This is due to uncontrolled rectifier is used in the secondary side to reduce the driving loss and maximum magnetic inductance also reduces the turn-off current of the switch. In particular, light or moderate loading efficiency is 1% higher than that in the literature [4], because the time domain analysis method is taken to obtain the maximum value of L_{m1}, which is independent of load change. The loss ratio i_{Lm1} increases under light load, so the efficiency increases greatly under light load. The oscillation at full load is significantly reduced, and the efficiency is increased.

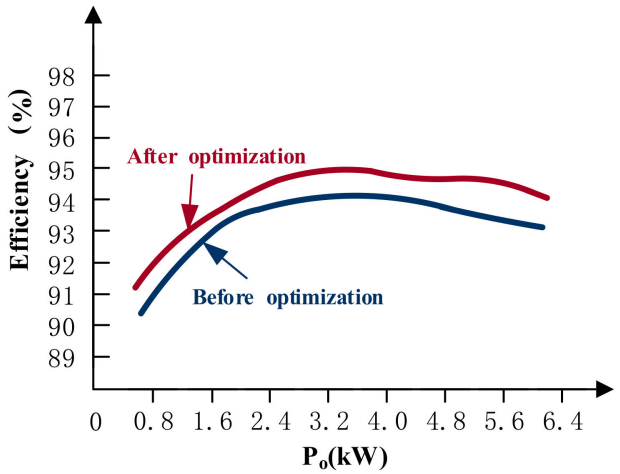

Figure 23. Operation efficiency of L-LLC-BDC under different load condition with forward transmission power.

The output voltage of the converter is constant by adjusting the frequency when the input voltage changes. The ideal switching frequency of the converter is 104 kHz when the input voltage is the rated voltage 760 V. The experiment waveforms are given in Figures 25–27 showing resonant current and output voltage at full load.

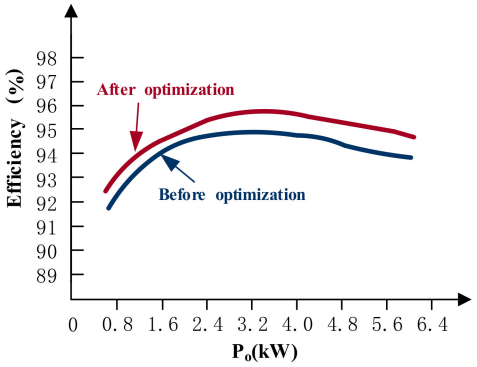

Figure 24. Operation efficiency of L-LLC-BDC under different load conditions with reverse transmission power.

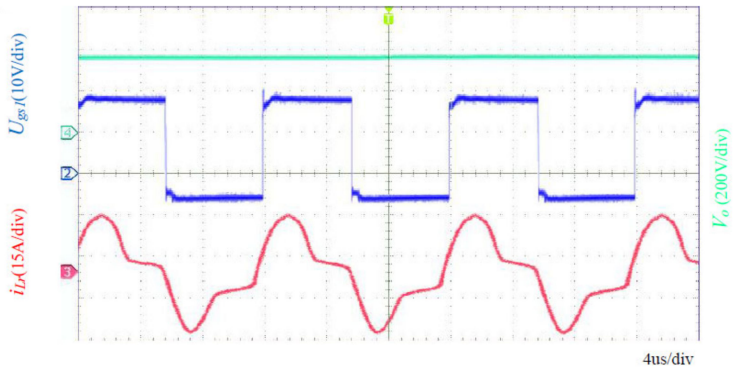

Figure 25. Experiment waveforms (V_{in} = 640 V).

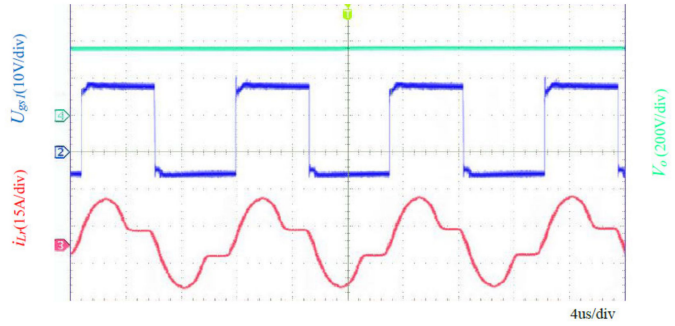

Figure 26. Experiment waveforms (V_{in} = 710 V).

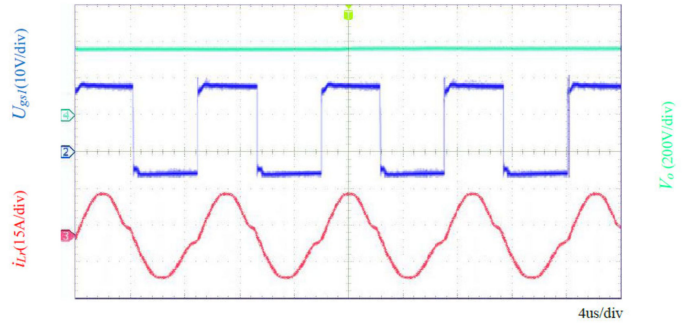

Figure 27. Experiment waveforms (V_{in} = 740 V).

The figures show that the optimized parameters in this paper can realize the closed-loop control of the converter by adjusting the frequency of the switch under different input voltages.

Figure 28 shows the operation efficiency of L-LLC-BDC resonant converter in forward mode under the different input voltage. The efficiency can reach up to 96% at rated power with an input voltage of 760 V.

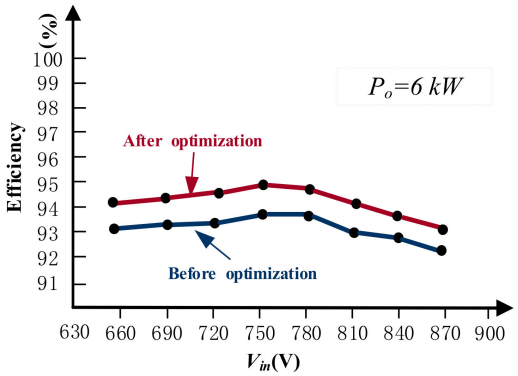

Figure 28. Operation efficiency of L-LLC-BDC resonant converter with forward transmission under different input voltage.

From reference [26], for the Sic device, the ratio of hysteresis energy loss E_{diss} and Coss stored energy E_{oss} is less than 0.1, even to 0.01. The device selected in this paper is C2M0080120D, E_{OSS} is 27 μJ when the input voltage is 760 V from the datasheet, so the maximum hysteresis energy loss E_{diss} is less than 2.7 μJ, even to 0.27 μJ, and maximum hysteresis loss of a single device is 0.27 W when the switching frequency is 100 kHz, even to 0.027 W. The proportion of the hysteresis loss is very small for the 6 kW converter.

Switching loss includes turn-on loss and turn-off loss. (1) Turn-on loss: The resonant converter achieves soft switching, which ideally yields zero losses, but various studies show that even if the soft switching is realized, there is hysteresis loss in the switch. The loss is very small by analysis quantitatively in the second question. (2) Turn-off loss: The turn-off loss of the switch in the primary side is about 2 W, turn-off loss of the switch in the secondary side ideally yields zero because the ZCS is realized when the converter operates at the main mode. In the actual state, C_{oss} transfers most loss to the conduction loss, However, the overall loss of the switch remains unchanged.

The main loss of the resonant converter is the conduction loss of the switch. The efficiency is improved because the current value passing through the switch of primary side is reduced in the design. Due to the large magnetic inductance of the transformer, the core loss of the transformer is slightly larger than that before optimization.

The power loss distribution and comparison of the before optimization and after optimization have been done and presented in Figure 29, and the loss breakdown has been down at full load and 760 V input.

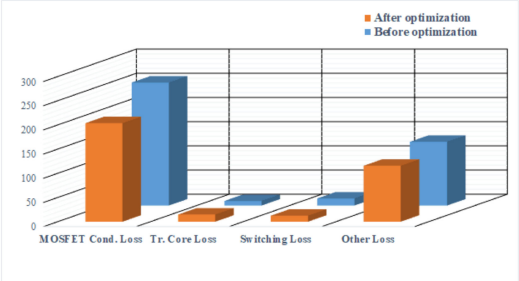

Figure 29. Power loss comparison between before optimization and after optimization of L-LLC-BDC.

6. Conclusions

For L-LLC resonant bidirectional DC-DC converter, with the effect of the output capacitance of the power device taken into account, a parameter optimization design method is proposed by configuring switching frequency and satisfying the gain range of the converter to achieve high efficiency.

Based on the complete charging and discharging of the output capacitance of the switch in the dead time, the magnetizing inductance is calculated. The configured switching frequency is calculated according to energy conservation law, and the inductance ratio satisfying the gain condition can be calculated according to the maximum voltage gain, and finally all the resonant parameters can be calculated. The experimental results show that the voltage and current oscillation is obviously eliminated, and the conduction and switching loss of the converter are reduced. The high efficiency can be ensured.

Author Contributions: Conceptualization, J.L. and X.T.; methodology, J.L.; software, J.L.; validation, J.L., M.S. and J.Y.; formal analysis, J.Z.; investigation, J.L.; resources, X.T.; data curation, J.L.; writing—original draft preparation, J.L. and J.Z.; writing—review and editing, J.L.; visualization, M.S.; supervision, X.T.; project administration, X.T.; funding acquisition, X.T. All authors have read and agreed to the published version of the manuscript.

Funding: This research was funded by the Natural Science Foundation of China, grant number 51677151.

Institutional Review Board Statement: Not applicable.

Informed Consent Statement: Not applicable.

Conflicts of Interest: The authors declare no conflict of interest.

Appendix A

The time domain equation when the converter operates at $f_s = f, f_s > f, f_s < f$, respectively. The subscript 1, 2 and 3 represent the converter operating at $f_s = f$, $f_s > f$ and $f_s < f$, respectively, N represents the normalized values of the physical quantities.

1. $f_s = f$

By normalizing all voltages with the voltage $U_N = nV_o$, and all currents with the current factor $I_N = nV_o/Z_r$.

$$\begin{cases} i_{Lr1N}(\omega t) = I_{Lr1N}\sin[\omega(t+t_{10})] \\ i_{P1N}(\omega t) = I_{P1N} + \frac{\omega t}{k} \\ u_{Cr1N}(\omega t) = -I_{Lr1N}\cos[\omega(t+t_{10})] + \frac{1}{M} - 1 \\ i_{Lm11N}(\omega t) = I_{Lm11N} + \frac{\omega t}{kM} \end{cases} \tag{A1}$$

where, Z_r is the characteristic impedance, $k = L_{m1}/L_r$, ω is resonance angle frequency, $\omega = 2\pi f$, M is the voltage gain, $M = nV_O/V_{in}$,$0 \le \omega t \le \omega t_1$, I_{Lr1N}, I_{Lm1N}, I_{P1N}, ωt, ωt_{10} and M are unknown quantities.

2. $f_s > f$

$$\begin{cases} i_{Lr2N}(\omega t) = I_{Lr2N}\sin[\omega(t+t_{20})] \\ i_{P2N}(\omega t) = I_{P2N} - \frac{\omega t}{k} \\ u_{Cr2N}(\omega t) = -I_{Lr2N}\cos[\omega(t+t_{20})] + \frac{1}{M} + 1 \\ i_{Lm12N}(\omega t) = I_{Lm12N} + \frac{\omega t}{kM} \end{cases} \tag{A2}$$

where, $0 \le \omega t \le \omega t_2$, I_{Lr2N}, I_{Lm12N}, I_{P2N}, ωt, ωt_{20}, and M are unknown quantities.

3. $f_s < f$

$$\begin{cases} i_{Lr3N}(\omega t) = i_{P3N} = I_{Lr3N}\sin[\omega(\sqrt{1/1+k}t + t_{30})] \\ i_{Lm13N}(\omega t) = I_{Lm13N} + \frac{\omega t}{kM} \\ u_{Cr3N}(\omega t) = -I_{Lr3N}\cos[\omega(\sqrt{1/1+k}t + t_{30})] + \frac{1}{M} \\ u_{Lm13N}(\omega t) = \frac{\frac{1}{M} - u_{Cr3N}(\omega t)}{1+k} \end{cases} \tag{A3}$$

where, $0 \le \omega t \le \omega t_3$, I_{Lr3N}, I_{LM13N}, ωt, ωt_{30} and M are unknown quantities, $u_{Lm13N}(\omega t)$ is the voltage of magnetizing inductance.

Stage indirect continuity condition:

$$\begin{cases} i_{Lr1N}[\omega(t+t_{10})] = i_{Lr3N}(0) \\ i_{Lm11N}[\omega(t+t_{10})] = i_{Lr3N}(0) \\ u_{Cr1N}[\omega(t+t_{10})] = u_{Cr3N}(0) \\ i_{P1N}[\omega(t+t_{10})] = i_{P3N}(0) \end{cases} \tag{A4}$$

$$\begin{cases} i_{Lr3N}[\omega(t+t_{30})] = i_{Lr3N}(0) \\ i_{Lm13N}[\omega(t+t_{30})] = i_{Lr3N}(0) \\ u_{Cr3N}[\omega(t+t_{30})] = u_{Cr3N}(0) \\ u_{Lm1N}[\omega(t+t_{30})] = -1 \\ i_{P3N}[\omega(t+t_{30})] = i_{P3N}(0) \end{cases} \tag{A5}$$

Symmetry condition of switching moment:

$$\begin{cases} i_{Lr1N}(0) = -i_{Lr2N}[\omega(t+t_{20})] \\ i_{Lr1N}(0) = -i_{Lm12N}[\omega(t+t_{20})] \\ u_{Cr1N}(0) = -u_{Cr2N}[\omega(t+t_{20})] \\ i_{P1N}(0) = -i_{P2N}[\omega(t+t_{20})] \end{cases} \tag{A6}$$

Modal phase angle satisfies the equation when working state is continuous under $f_s = f, f_s > f$ and $f_s < f$ is:

$$\omega(t+t_{10}) + \omega(t+t_{20}) + \omega(t+t_{30}) = \frac{f_s \pi}{f} \tag{A7}$$

The zero current peak gain is:

$$i_{Lr1N}(0) = i_{Lr2N}[\omega(t+t_{20})] = 0 \tag{A8}$$

Given the minimum switching frequency f_s, peak gain M and other unknown parameters can be solved.

References

1. Jiang, T.; Zhang, J.; Wu, X. Bidirectional LLC resonant converter with synchronous control method. *Trans. China Electro Tech. Soc.* **2015**, *30*, 87–96.
2. Jiang, T.; Zhang, J.; Wu, X. A Bidirectional LLC resonant converter with automatic forward and back mode transition. *IEEE Trans. Power Electron.* **2015**, *30*, 757–770. [CrossRef]
3. Chen, Q.; Ji, Y.; Wang, J. Analysis and design of bidirectional CLLC resonant DC-DC transformers. *Proc. CSEE* **2014**, *34*, 2898–2905.
4. Lv, Z.; Yan, X.; Sun, L. A L-LLC resonant bidirectional DC-DC converter based on hybrid control of variable frequency and phase shift. *Trans. China Electrotech. Soc.* **2017**, *32*, 12–24.
5. Lee, I. Hybrid DC–DC Converter with Phase-Shift or Frequency Modulation for NEV Battery Charger. *IEEE Trans. Ind. Electron.* **2016**, *63*, 884–893. [CrossRef]

6. Wei, Y.; Fred, C.L.; Mattavelli, P. Optimal Trajectory Control of Burst Mode for LLC Resonant Converter. *IEEE Trans. Power Electron.* **2013**, *28*, 457–466.
7. Shi, L.; Liu, B.; Duan, S. Burst-Mode and Phase-Shift Hybrid Control Method of LLC Converters for Wide Output Range Applications. *IEEE Trans. Ind. Electron.* **2020**, *67*, 1013–1023. [CrossRef]
8. Ren, R.; Zhang, F.; Liu, S. Optimal design for Efficiency based on the dead time and magnetizing inductance of LLC DC transformer. *Trans. China Electrotech. Soc.* **2014**, *29*, 141–146.
9. Hu, H.; Wang, W.; Sun, W.; Ding, S.; Xing, Y. Optimal efficiency design of LLC resonant converter. *Proc. CSEE* **2013**, *33*, 48–56.
10. Fang, X.; Hu, H.; Shen, J.; Batarseh, I. Operation Mode Analysis and Peak Gain Approximation of the LLC Resonant Converter. *IEEE Trans. Power Electron.* **2012**, *27*, 1985–1995. [CrossRef]
11. Hu, Z.; Wang, L.; Wang, H.; Liu, Y.; Sen, P.C. An Accurate Design Algorithm for LLC Resonant Converters-Part I. *IEEE Trans. Power Electron.* **2016**, *31*, 5435–5447. [CrossRef]
12. Hu, Z.; Wang, L.; Wang, H.; Liu, Y.; Sen, P.C. An Accurate Design Algorithm for LLC Resonant Converters—Part II. *IEEE Trans. Power Electron.* **2016**, *31*, 5448–5460. [CrossRef]
13. Liu, J.; Zhang, J.; Zheng, T.Q.; Yang, J. A Modified Gain Model and the Corresponding Design Method for an LLC Resonant Converter. *IEEE Trans. Power Electron.* **2017**, *32*, 6716–6727. [CrossRef]
14. Lee, B.H.; Kim, M.Y.; Kim, C.E. Analysis of LLC resonant converter considering effects of parasitic components. In Proceedings of the INTELEC 2009—31st International Telecommunications Energy Conference, Incheon, Korea, 18–22 October 2009; pp. 1–6.
15. Musavi, F.; Craciun, M.; Edington, M.; Eberle, W.; Dunford, W.G. Practical design considerations for a LLC multi-resonant DC-DC converter in battery charging applications. In Proceedings of the 2012 Twenty-Seventh Annual IEEE Applied Power Electronics Conference and Exposition (APEC), Orlando, FL, USA, 5–9 February 2012; pp. 2596–2602.
16. Shafiei, N.; Ordonez, M.; Craciun, M.; Botting, C.; Edington, M. Burst Mode Elimination in High-Power LLC Resonant Battery Charger for Electric Vehicles. *IEEE Trans. Power Electron.* **2016**, *31*, 1173–1188. [CrossRef]
17. Wang, D.; Zhang, P.; Jin, Y.; Wang, M.; Liu, G.; Wang, M. Influences on Output Distortion in Voltage Source Inverter Caused by Power Devices' Parasitic Capacitance. *IEEE Trans. Power Electron.* **2018**, *33*, 4261–4273. [CrossRef]
18. Kim, J.H.; Kim, C.E.; Kim, J.K.; Moon, G.W. Analysis for LLC resonant converter considering parasitic components at very light load condition. In Proceedings of the 8th International Conference on Power Electronics—ECCE Asia, Jeju, Korea, 30 May–3 June 2011; pp. 1863–1868.
19. Park, K.B.; Lee, B.H.; Moon, G.W.; Youn, M.J. Analysis on Center-Tap Rectifier Voltage Oscillation of LLC Resonant Converter. *IEEE Trans. Power Electron.* **2012**, *27*, 2684–2689. [CrossRef]
20. Zhao, X.; Zhang, L.; Born, R.; Lai, J.-S. A High-Efficiency Hybrid Resonant Converter with Wide-Input Regulation for Photovoltaic Applications. *IEEE Trans. Ind. Electron.* **2017**, *64*, 3684–3695. [CrossRef]
21. Chen, W.; Rong, P.; Lu, Z. Snubberless Bidirectional DC–DC Converter with New CLLC Resonant Tank Featuring Minimized Switching Loss. *IEEE Trans. Ind. Electron.* **2010**, *57*, 3075–3086. [CrossRef]
22. Jung, J.H.; Kim, H.S.; Ryu, M.H.; Baek, J.W. Design Methodology of Bidirectional CLLC Resonant Converter for High-Frequency Isolation of DC Distribution Systems. *IEEE Trans. Power Electron.* **2013**, *28*, 1741–1755. [CrossRef]
23. Chen, Q.; Ji, Y.; Wang, J.; Pan, Y.; Ma, C. Analysis of the influence of MOSFET output capacitance on the bidirectional CLLC resonant converter. *Trans. China Electrotech. Soc.* **2015**, *30*, 26–35.
24. Lv, Z.; Yan, X. Mode analysis and optimal design of CLLC-type Bidirectional DC-DC transformers for high-frequency isolation in DC nanogrids. *Proc. CSEE* **2016**, *36*, 5918–5929.
25. Menke, M.F.; Seidel, A.R.; Tambara, R.V. LLC LED Driver Small-Signal Modeling and Digital Control Design for Active Ripple Compensation. *IEEE Trans. Ind. Electron.* **2019**, *66*, 387–396. [CrossRef]
26. Perera, N.; Jafari, A.; Nela, L.; Kampitsis, G.; Nikoo, M.S.; Matioli, E. Output-Capacitance Hysteresis Losses of Field-Effect Transistors. In Proceedings of the 2020 IEEE 21st Workshop on Control and Modeling for Power Electronics (COMPEL), Aalborg, Denmark, 9–12 November 2020; pp. 1–8.